

## RESEARCH ARTICLE

10.1029/2018JC014113

## Key Points:

- Anthropogenic aerosol deposition is the dominant source of most particulate trace metals collected in the surface water of the Kuroshio
- The distribution patterns of particulate metal composition in the global surface water are associated with aerosol deposition fluxes
- The distribution patterns of particulate metal composition validate intracellular trace metal stoichiometry concept in plankton

## Supporting Information:

- Supporting Information S1
- Data Set S1

## Correspondence to:

T.-Y. Ho,  
tyho@gate.sinica.edu.tw

## Citation:

Liao, W.-H., & Ho, T.-Y. (2018). Particulate trace metal composition and sources in the Kuroshio adjacent to the East China Sea: The importance of aerosol deposition. *Journal of Geophysical Research: Oceans*, 123. <https://doi.org/10.1029/2018JC014113>

Received 25 APR 2018

Accepted 9 AUG 2018

Accepted article online 22 AUG 2018

## Particulate Trace Metal Composition and Sources in the Kuroshio Adjacent to the East China Sea: The Importance of Aerosol Deposition

Wen-Hsuan Liao<sup>1,2,3</sup> and Tung-Yuan Ho<sup>1,2,3,4</sup> 

<sup>1</sup>Research Center for Environmental Changes, Academia Sinica, Taipei, Taiwan, <sup>2</sup>Earth System Science Program, Taiwan International Graduate Program, Academia Sinica, Taipei, Taiwan, <sup>3</sup>College of Earth Sciences, National Central University, Taoyuan, Taiwan, <sup>4</sup>Institute of Oceanography, National Taiwan University, Taipei, Taiwan

**Abstract** The Kuroshio, flowing through the eastern end of the East China Sea, transports terrestrial material to the Northwestern Pacific Ocean. Along the Kuroshio path, we collected size-fractionated suspended particles in the upper 200 m to investigate the composition and sources of particulate trace metals. Demonstrated by Al- and P-normalized elemental ratios, we found that anthropogenic aerosol deposition was the major source of most particulate trace metals in the Kuroshio region although the impact of bottom resuspension and riverine input may be significant at some specific regions. As seen in our previous studies in the South China Sea and the Western Philippine Sea, this study concluded that anthropogenic aerosol deposition is the dominant particulate trace metal source in the surface water of the Northwestern Pacific Ocean and its marginal seas. Compared to particulate trace metal composition obtained in other open oceans, we found that the distribution patterns of particulate trace metal composition in the surface waters are closely associated with aerosol deposition fluxes. In regions with low deposition, the particulate trace metal concentrations were extremely low and metal to P ratios were all comparable to their intracellular quota previously proposed. In regions with high deposition, metal to P ratios were highly elevated in comparison to their intracellular quota and metal to Al ratios were deviated from lithogenic ratios to various extents. The globally consistent distribution patterns validate trace metal stoichiometry concept in plankton intracellularly and the primary role of aerosol deposition on deciding particulate trace metal composition in oceanic surface water globally.

**Plain Language Summary** The Kuroshio adjacent to the East China Sea is an ideal region to investigate the material exchange and transport from the marginal sea to the Northwestern Pacific Ocean. Particulate trace metals may serve as useful proxies or tracers for the sources of particulate materials in the Kuroshio and material exchange with the marginal seas and islands. In addition to aerosol transport, both anthropogenic and lithogenic materials carried by riverine or sediment transport may be additional sources of particulate trace metals in the studied region. In this study, we found that anthropogenic aerosol deposition is the dominant particulate trace metal source in the surface water. Compared to the data obtained in other open oceans, we further revealed that the distribution patterns of particulate trace metal composition in the surface waters are closely associated with aerosol deposition globally. The globally consistent distribution patterns also validate that plankton possess relatively constrained trace metal composition intracellularly.

### 1. Introduction

The Kuroshio, originating from the northward bifurcation of the North Equatorial Current, transports large amounts of water mass, heat, and particulate materials from the equatorial Pacific to the Northwestern Pacific Ocean (NWPO) in a current that is around 800 m deep and 100 km wide (Chao, 1991; Hsin et al., 2008; Jan et al., 2015). The Kuroshio passes the eastern coast of Luzon, the Luzon Strait, the eastern end of Taiwan, the shelf edge of the East China Sea (ECS), the southeast coast of Kyushu, then to the NWPO. The Kuroshio dynamically exchanges seawater and particulate material with the two marginal seas, the ECS and the South China Sea (SCS), and receives terrestrial discharge from Luzon, Taiwan, East China, and various islands. As the ECS is located next to the most populated region of China, the marginal sea receives a significant amount of anthropogenic and lithogenic material from many terrestrial sources (Hsu et al., 2010; Ren et al., 2015). The Kuroshio adjacent to the ECS is thus an ideal region to investigate the material exchange and transport from the marginal sea to the Kuroshio and the NWPO. Particulate trace metals

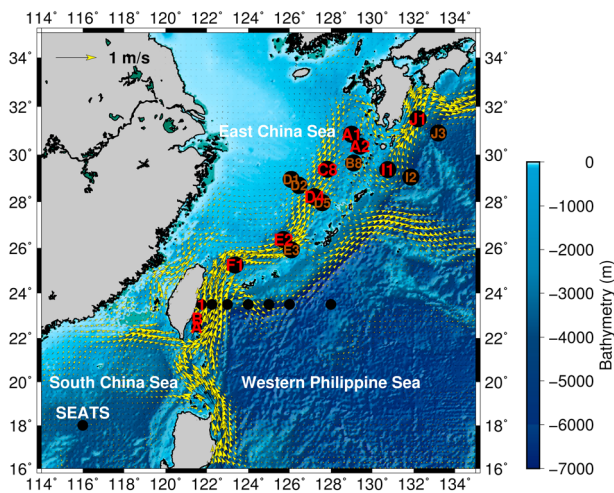


**Figure 1.** The sampling stations in this study and the main stream of the Kuroshio current. The annual average geostrophic velocity in the top 50 m was derived from a numerical study (Hsin et al., 2008). The data, obtained from our previous study in November 2013 (Liao et al., 2017), from stations A, B, and 1, were also included in this study for comparison.

anthropogenic aerosol deposition is the dominant source of particulate trace metal in the surface water of the SCS and the Western Philippine Sea (WPS; Ho et al., 2007; Liao et al., 2017). The role of aerosol deposition in the Kuroshio region can be significant due to the proximity of East Asia. However, introduction of anthropogenic and lithogenic materials by riverine or sediment transport may be additional important sources of particulate trace metals in the Kuroshio water adjacent to the ECS. Horizontal transport of trace metals originating from continental shelves can also be a major particulate trace metal source to the water column of remote open ocean regions (Lam & Bishop, 2008). In this study, size-fractionated particulate samples were collected along the Kuroshio path adjacent to the ECS from Taiwan to Southern Japan (Figure 1). The sources of particulate trace metals along the path were investigated using their spatial distribution and elemental ratios. The fluxes of particulate trace metals transported along the path of the Kuroshio were also quantified.

## 2. Materials and Methods

Size-fractionated particulate samples were collected during the Japanese GEOTRACES cruise KH-15-3, conducted by the R/V Hakuho-Maru in October 2015. The sampling sites are shown in Figure 1 and Table S1 in the supporting information. Seawater for particle samples was collected in the top 200 m of the sampling stations using acid-washed 12-L Teflon-coated Niskin-X bottles mounted on a Teflon-coated rosette deployed with titanium hydrowires. A trace metal clean filtration apparatus equipped with 150-, 60-, and 10- $\mu\text{m}$  aperture changeable Nitex nets in sequence was used to gently separate and collect different sizes of suspended particle samples by gravity filtration (Ho et al., 2007; Wen et al., 2018). Seventy-two to 96 L of seawater were filtered depending on the sampling arrangement. Subsequently, approximately 5–10 L of seawater were filtered through the 10- $\mu\text{m}$  net to obtain the size fraction ranging from 0.2 to 10  $\mu\text{m}$ . Polycarbonate membranes (Millipore) with 10- $\mu\text{m}$  pore size were used to collect particles in the size fractions of 10–60, 60–150, and > 150  $\mu\text{m}$ , and 0.2- $\mu\text{m}$  polyethersulfone membrane filters (Sterlitech) were used to collect the 0.2- to 10- $\mu\text{m}$  fraction. Filtration vacuum pressure was kept lower than 2.2 psi (15 kPa) to avoid particle breakup. After filtration, all of the membranes with particles were quickly misted and rinsed with Milli-Q water three times to remove seawater residue to reduce the interference of sea salts on trace metal analysis by inductively coupled plasma mass spectrometer (ICPMS). Then all the membranes were immediately sealed in 7-ml Teflon vials and brought back to land-based laboratory for further treatment and analysis. The sampling procedures and the description of the filtration device are described in details in our previous studies (Ho et al., 2007; Liao et al., 2017).

The membranes with particles were digested with 5-ml 8 N  $\text{HNO}_3$  and 2.9 N HF mixture in the Teflon vials at 120  $^\circ\text{C}$  for 12 hr on a hot plate in a laminar flow bench of a clean laboratory. After digestion, we used Milli-Q

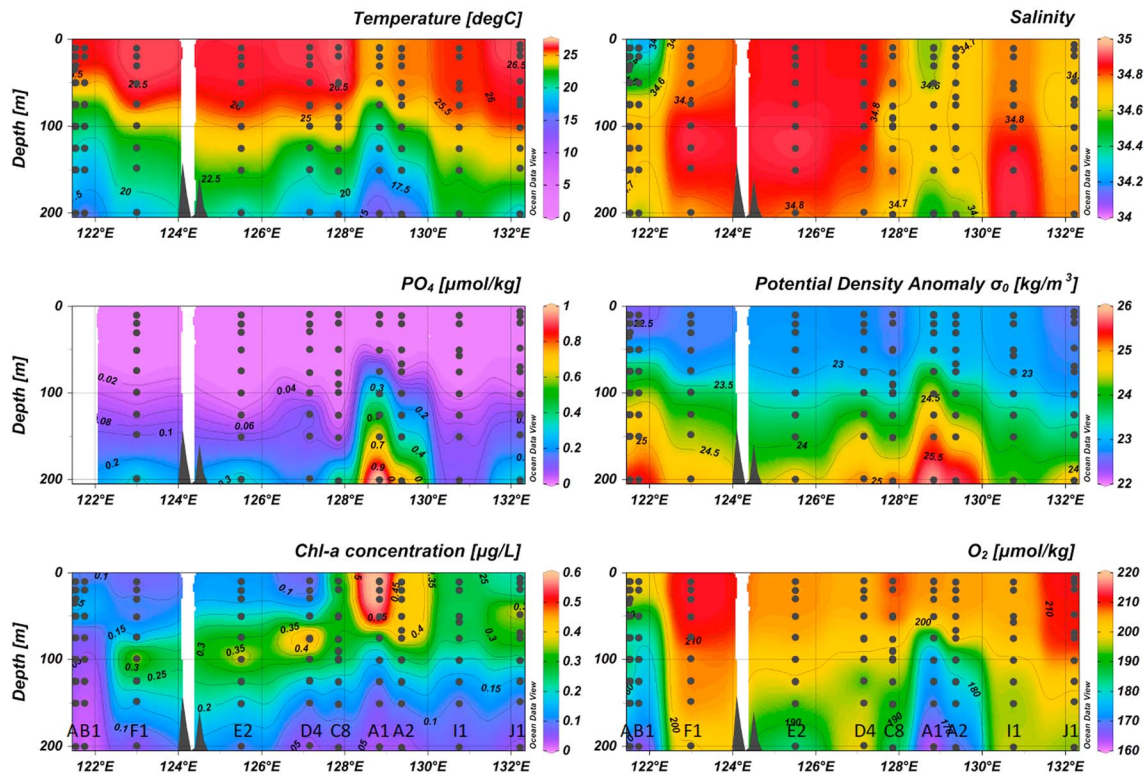


**Figure 2.** The transects of some basic hydrographic parameters along the Kuroshio path from east of Taiwan to south of Kyushu. The stations are labeled at the bottoms of the Chl *a* and oxygen contours.

water to rinse the membranes and collect the residue liquid on membranes in the digestion vials. The digestion solutions were evaporated to dryness on a hot plate in a trace metal clean hood. The dried samples were redissolved in 1-ml concentrated super pure HNO<sub>3</sub> and evaporated again to dryness. The dried samples were redissolved and diluted by adding 0.5 N super pure HNO<sub>3</sub> for trace metal analysis by ICPMS. All elemental concentrations reported were analyzed by a sector field high-resolution ICPMS (Thermo Fisher Scientific, Element XR), which was executed with a SC-Fast autosampler (Elemental Scientific) and an Apex HF-Spiro membrane desolvation device (Elemental Scientific) to reduce oxide interferences. The details for the precision, accuracy, and detection limits of the method were described previously (Ho et al., 2007; Liao et al., 2017). The overall procedure blanks, detection limits, and the recovery of the reference material (BCR-414) obtained in this study were consistent with results reported in Liao et al. (2017). In addition to the validation of the reference material, our laboratory also obtained reliable results during the GEOTRACES particulate trace metal intercalibration study, which included relatively low mass particulate samples collected at both coastal and open ocean locations (Phoebe Lam, personal communication, March 29, 2016).

The hydrographic parameters, chlorophyll *a* (Chl *a*) and dissolved oxygen concentrations were measured by fluorometer (Seapoint) and SBE-43 sensors (Sea Bird Electronics) mounted on the conductivity-temperature-depth frame. The dissolved oxygen concentrations were calibrated by the Winkler method on discrete samples. Nutrient concentrations were measured on board by using a SWAAT auto-analyzer (BL-TEC Japan) right after sampling. Detection limits for measurement of nitrate and nitrite, phosphate, and silicate were 0.05, 0.11, and 0.03 μM, respectively. Quality control of nutrient analysis was validated by reference material (KANSO). Phosphate concentrations are shown as representative of nutrient distributions along the Kuroshio path (Figure 2).

### 3. Hydrographic and Physical Features

The Kuroshio, the strongest western boundary current in the North Pacific Ocean, is highly dynamic temporally and spatially. The details of its circulation pattern can be found in previous studies (Atkinson,

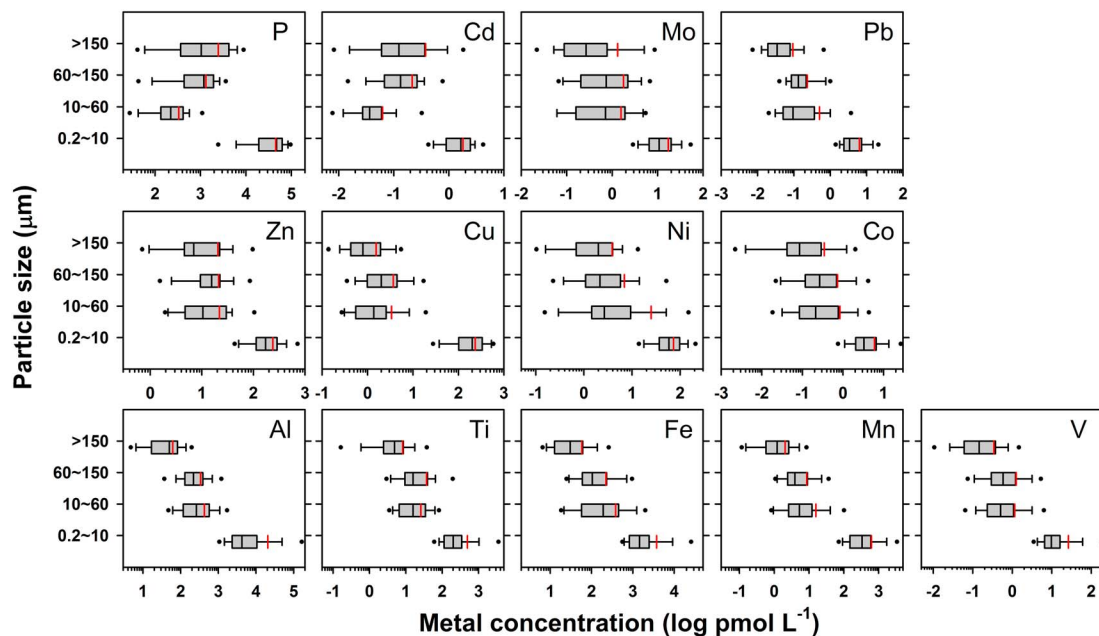


**Figure 3.** The distribution of size-fractionated particulate trace metal concentrations in seawater in the Kuroshio region. The ends of boxes and whiskers represent the 25th and 75th percentiles and the 5th and 95th percentiles, respectively. The black and red lines stand for the median and mean, respectively. Black solid points are the maximum and minimum numbers.

2010; Chao, 1991; Hsin et al., 2008; Jan et al., 2015). The path and typical annual flow rates of the Kuroshio in the top 50 m, computed by a numerical study (Hsin et al., 2008), are shown in Figure 1. The vertical variations of the transect of major hydrographic parameters are presented in Figure 2, which include temperature, salinity, potential density anomaly, dissolved oxygen, Chl *a*, and phosphate concentrations. An upwelling feature was observed around the relatively shallow stations C8, A1, and A2, where all the parameters show an upwelling pattern in the subsurface water, including low temperature, salinity, and dissolved oxygen concentrations and elevated potential density, and phosphate and Chl *a* concentrations. These stations are located at the southern end of Kyushu, in the Tokara strait, where the Kuroshio turns right due to the abrupt topography shallowing and thus cause intensive turbulent mixing (Hasegawa et al., 2008; Tsutsumi et al., 2017). Indeed, abrupt shallowing of topography along the Kuroshio path is a major cause of strong vertical turbulent mixing (Chang et al., 2013; Tsutsumi et al., 2017). Although horizontal intrusion of coastal seawater may also play a role on the hydrographic variations within the Kuroshio, the study of Tsutsumi et al. (2017) found that vertical turbulent mixing is much more significant than the horizontal input. A similar upwelling feature was also observed at stations A, B, and 1, where the Kuroshio flows through Green Island, Taiwan. Chang et al. (2013) also observed cold eddy formation in the wake of Green Island, which may also enhance Chl *a* concentrations. In addition to the influence on water masses and the hydrographic parameters, turbulent mixing also affects the distribution of particulate material at the studied stations.

#### 4. Particulate Trace Metal Distribution Patterns

As shown in Figure 3, total particulate trace metal concentrations in seawater varied significantly among the four different size fractions, with concentration ranging from  $10^{-3}$  to  $10^5$  pmol/L in the sequence of  $P > Al > Fe > Ti-Mn-Zn-Cu > V-Mo > Co > Cd$ . Despite of the enormous concentration variations, distribution patterns of the size-fractionated concentrations exist among the elements (Figure 3). Overall, the concentrations in the 0.2- to 10- $\mu$ m fraction account for over 80% of total concentrations for most of the particulate samples. P and Cd, which have highest concentrations in the 0.2- to 10- $\mu$ m fraction, possess lowest concentrations in 10- to 60- $\mu$ m fraction, which were significantly lower than other fractions ( $p < 0.01$ ). The elements, Al, Ti, Fe, Mn, and V, exhibit the lowest concentrations in the largest fraction. For these

elements, the concentrations between 10- to 60- and 60- to 150- $\mu\text{m}$  fractions were not statistically different ( $p > 0.01$ ), but they were significantly higher than the largest fraction ( $p < 0.01$ ). The third pattern, containing Co, Ni, Cu, Zn, Mo, and Pb, shows similar concentration ranges among the three relatively large fractions ( $p > 0.01$ ). The  $p$  values of the statistical analysis were listed in the supporting information Excel file. As the three larger size fractions accounted for a minor portion of the total particulate concentrations in seawater, we have categorized the four size data into two fractions to simplify the presentation of size-fractionated particulate trace metal distribution patterns, the concentrations in the small size fraction (SSF, 0.2–10  $\mu\text{m}$ ) and the large size fraction (LSF, the fractions larger than 10  $\mu\text{m}$ ) for further discussion.

The vertical distributions of the particulate trace metal concentrations in the SSF and the LSF along the Kuroshio path are shown in Figures 4 and 5, respectively. For the SSF, P and Cd have relatively similar distribution patterns as Chl *a* shown in Figure 2. The elevated concentrations for P, Cd, and Chl *a* were generally located in the top 100 m, particularly noticeable around the upwelling region or the stations C8, A1, and A2. The elements on the right panel, including Al, Ti, Fe, Mn, Co, and V, exhibited a similar distribution pattern with hydrographic parameters around the upwelling region (Figure 2). The Kuroshio turns right due to the abrupt topography shallowing and thus causes intensive turbulent mixing, which further induces bottom sedimentary resuspension and results in elevated particulate trace metal concentrations. Hybrid distributions were observed for Ni, Cu, and Zn, which showed similarity with both P and Al to different extents. The elemental ratios of these three elements also exhibited the hybrid feature for both biotic and abiotic materials in our previous studies in the SCS and WPS (Ho et al., 2007; Liao et al., 2017). Mo distribution generally showed a distribution pattern closer to lithogenic type elements but possessed some elevated concentrations in the top 100 m. The distribution of Pb displayed elevated concentrations at the upwelling region and the coastal stations close to the Green Island, Taiwan.

In the LSF, the concentrations of almost all elements displayed high value in the upwelling region. The distribution of Cd and P showed a slightly different pattern between the LSF and SSF, which may be due to differential uptake of Cd between small and large phytoplankton. The elevated concentrations of Al and Ti in the LSF were also observed at the upwelling region, particularly at station C8. Similarly, the elements, Fe, Mn, Co, V, Ni, Cu, and Mo, also exhibited elevated concentrations between 50 and 100 m at station C8. The distribution of Pb in the LSF exhibited elevated concentrations at stations near Taiwan, but there were no elevated values observed in the upwelling region. The distribution of Mo shows elevated concentrations in the middle of the path, ranging from the stations E2 and A2. The percentage of the LSF concentrations to total particulate concentrations is presented in Figure S1. The major difference is that the fraction of Mo in the LSF is high in the middle of the Kuroshio path adjacent to the ECS. The elevated Mo concentrations in the LSF may be related to *Trichodesmium* as nitrogenase is a Mo-dependent enzyme and *Trichodesmium* is a major diazotroph around the Ryukyu Islands (Shiozaki et al., 2015).

The concentration correlations and potential sources of the elements were further evaluated by principal component analysis (PCA). The data are derived from 192 samples collected from the surface water of the 18 stations (Table S1). The values of Kaiser-Meyer-Olkin test are 0.70, 0.74, and 0.83, for the SSF, LSF, and total amount, respectively, indicating the sampling of our PCA was adequate (Table S2). The four samples from the upwelling region with abnormally high concentrations were not included in the PCA to reduce bias. The PCA results show that three principle components explain 81, 72, and 82% of total variance for the concentrations in the SSF, the LSF, and total concentrations, respectively; and 48, 24, and 9%; 36, 25, and 11%; and 59, 16, and 7% of individual variance of the first three major components for the SSF, the LSF, and total amount, respectively. The factor scores of each element are listed in Table S2, showing the correlation of each element to the major components. The first major component for the SSF mainly explain the variance of the elements P, Cd, Mo, Mn, Ni, and Co, suggesting that PC1 is a biotic particle related component (Figure 6). The variations of Al, Ti, Fe, and V were mainly controlled by second component, mostly likely to be associated with lithogenic material. The third component explains considerable percentage of the concentration variance of Co, Ni, Cu, Zn, and Pb, suggesting that the component is possibly associated with anthropogenic material. Further discussion for these metals originated from anthropogenic aerosols is presented in section 6. For the LSF, the first major component mainly explains the variance of Fe, Co, Ni, and Cu. The second component, including P, Cd, Zn, and Mo, is most likely to be associated with biogenic materials. Overall, the PCA results for total concentrations are closer to the results of the SSF than LSF. The major differences for the PCA results between the SSF and total concentrations are about the factors explaining the variance of Co, Ni, Cu, and Zn.

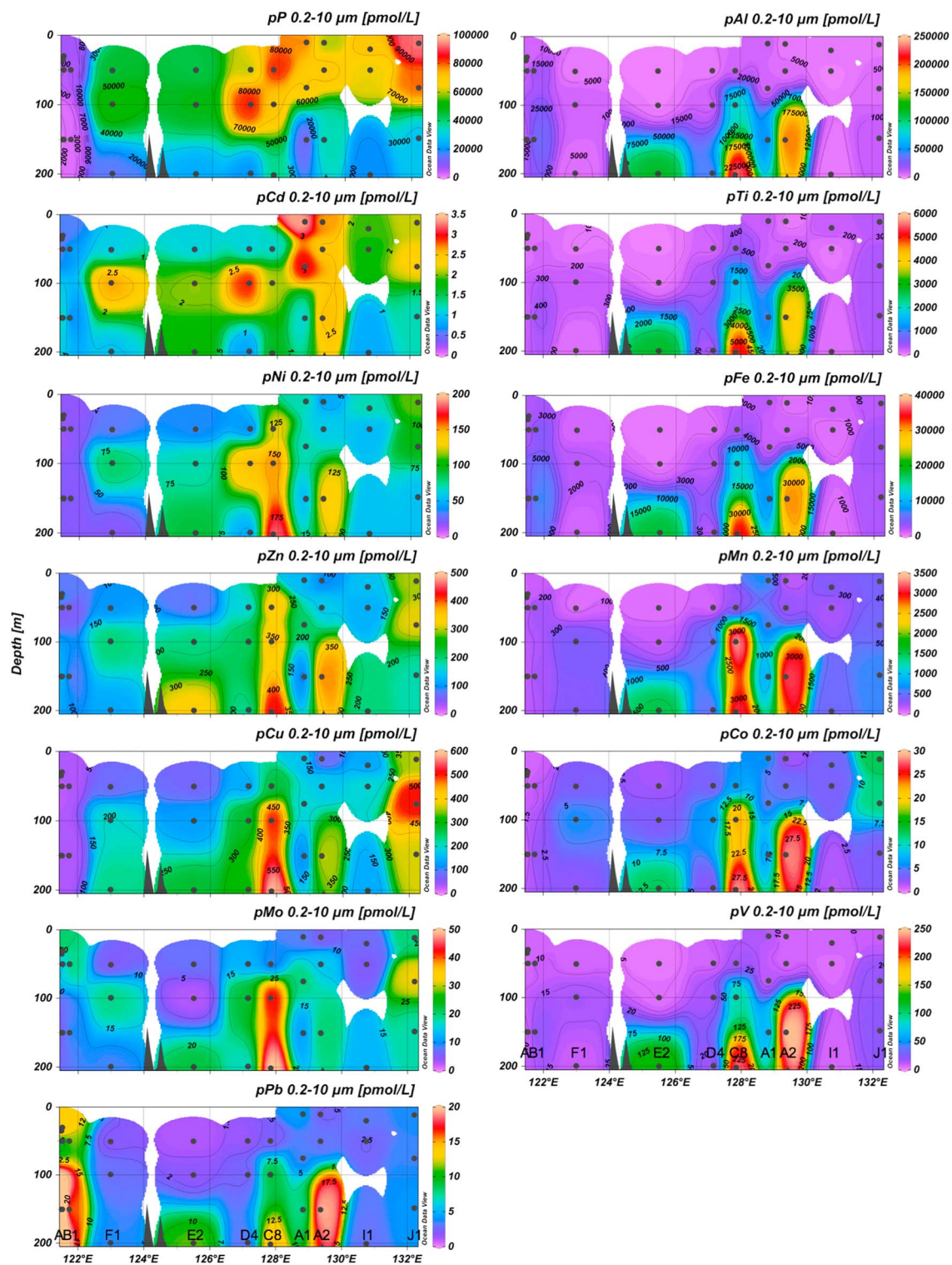


**Figure 4.** The distribution of small size fraction (0.2–10  $\mu\text{m}$ ) trace metal concentrations in seawater along the Kuroshio path, from east of Taiwan to south of Kyusyu (from left to right).

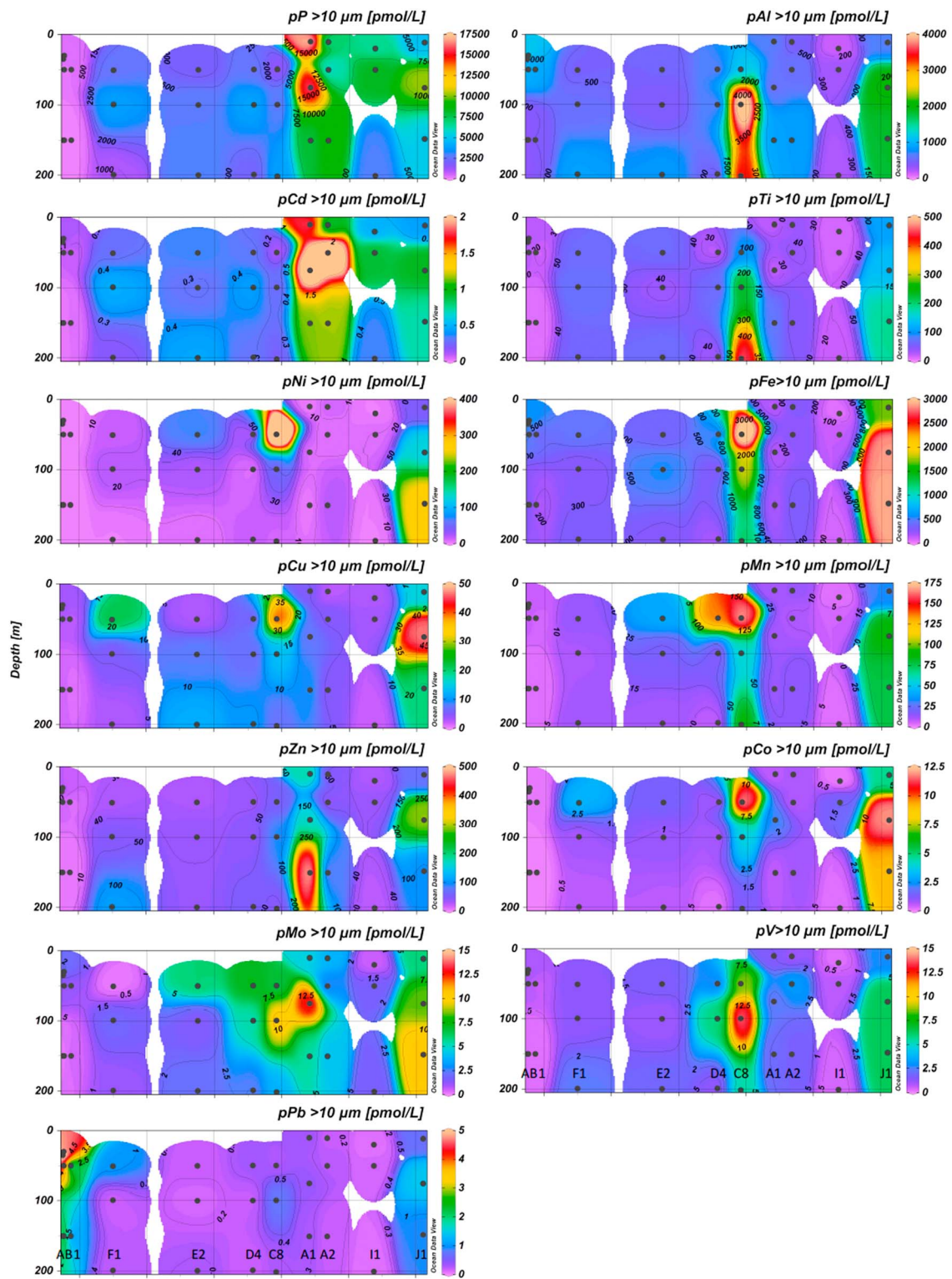


**Figure 5.** The distribution of large size fraction (>10 μm) trace metal concentrations in seawater along the Kuroshio path.

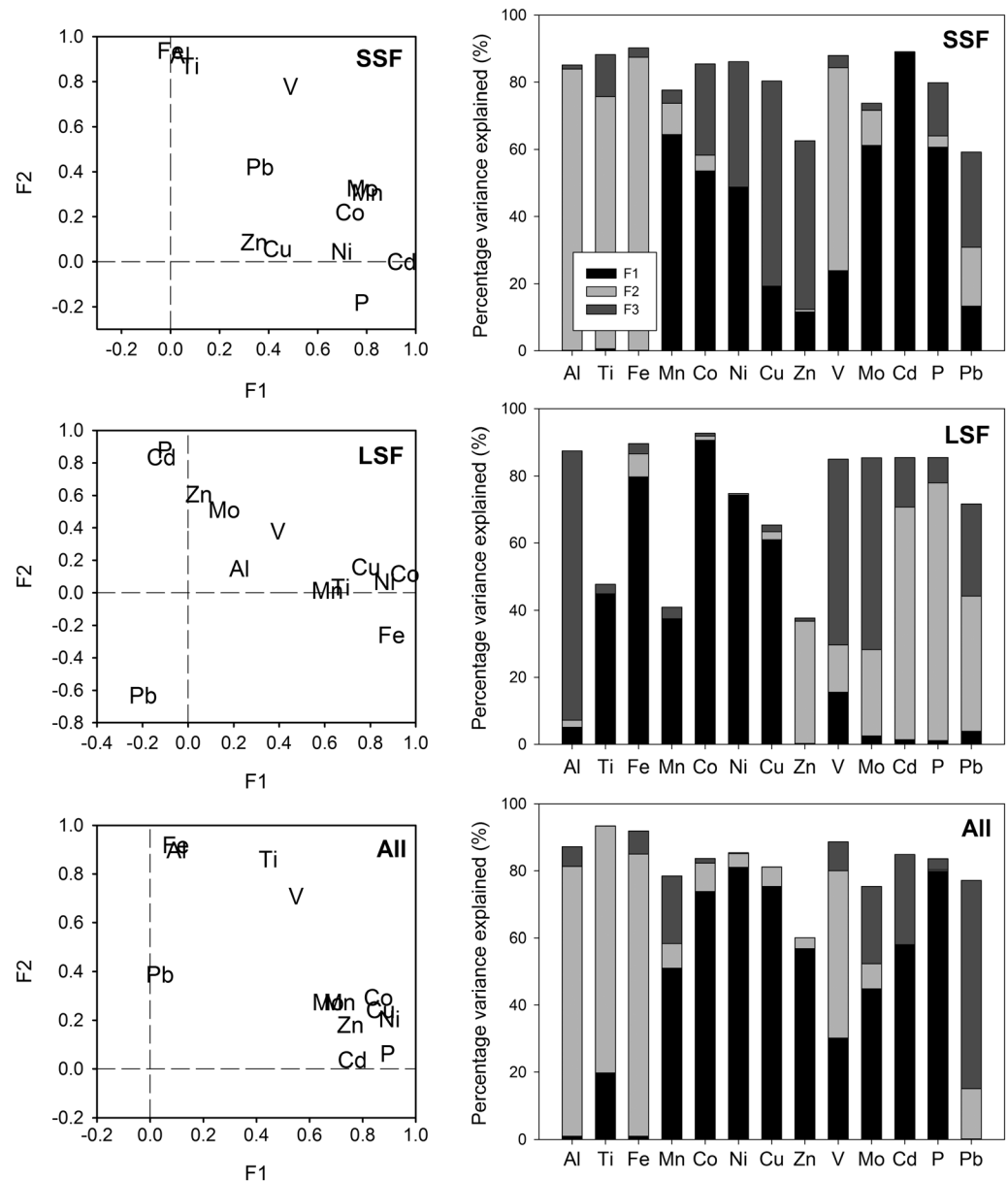


**Figure 6.** The results of principal components analysis of particulate elemental concentrations in the SSF, the LSF, and total concentrations. F1, F2, and F3 stand for the first three major components. The correlations of elements are shown in the left panels; the variances explained by the three major components are shown in the right panels. The analyses were carried out by statistical product and service solutions 12. The four abnormally high concentration data obtained from the upwelling region were not included in the calculation to reduce bias. SSF = small size fraction; LSF = large size fraction.

### 5. Particulate Trace Metal Fluxes Along the Kuroshio Path

The Kuroshio downstream water mass transport generally ranges from 14.7 to 16.7 Sv in the upper 250 m along the path from Eastern Taiwan to Southern Kyushu, accounting for over 50% of the total transport above 1,000 m (Chen et al., 2017; Guo et al., 2013). In addition to water mass and heat, the transport also carries dissolved and particulate major and minor nutrients along the flowing path to the NWPO (Figure 1). For example, nitrate transport was previously estimated by multiplying nitrate concentrations times the water mass fluxes along the Kuroshio path (Chen et al., 2017). Here we estimated particulate trace metal fluxes by multiplying average particulate trace metal concentrations obtained at stations 3 (Liao et al., 2017), D4, I1, and J1 (this study) with upper 250-m water mass fluxes obtained from previous studies at various sections

**Table 1**  
*The Estimated Fluxes of Dissolved and Particulate Trace Metals Transported Along the Kuroshio Path*

Flux (mol/s)	Cd	Pb	Al	P	Ti	V	Mn	Fe	Co	Ni	Cu	Zn	Mo
Dissolved Kuroshio <sup>a</sup>	0.34	1.23	228 <sup>b</sup>	1600 <sup>c</sup>	—	—	23	82 <sup>d</sup>	0.21	35	17	25	—
Particulate													
KTV <sup>e</sup>	0.007	0.14	95	78	1.9	0.19	1.3	69	0.02	0.4	0.5	0.8	0.16
PN <sup>f</sup>	0.033	0.04	89	966	4.8	0.25	6.3	27	0.07	1.5	4.1	3.8	0.37
TK <sup>f</sup>	0.033	0.05	50	878	2.7	0.12	5.4	17	0.05	1.0	2.5	2.8	0.15
ASUKA <sup>f</sup>	0.038	0.07	123	1083	7.0	0.33	8.0	73	0.26	3.5	6.5	6.2	0.47

Note. The uncertainties of the fluxes generally range from 14% to 53%, which are not shown here to simplify the expression.

<sup>a</sup>The dissolved trace metal concentrations (Cd, Pb, Mn, Co, Ni, Cu, and Zn) were obtained near Kuroshio region, east of Taiwan (Wang et al., 2014). <sup>b</sup>Average Al concentrations was obtained near station C9 (Ren et al., 2015). <sup>c</sup>Dissolved particulate phosphorus fluxes were estimated from nitrate fluxes using the Redfield ratio (Chen et al., 2017). <sup>d</sup>Fe concentrations in top 200 m were obtained at station P12 of the study (Su et al., 2015). <sup>e</sup>The KTV transect is near station 3 (Jan et al., 2015). <sup>f</sup>The three transects (PN, TK, and ASUKA) are near stations D4, I1, and J1, respectively (Guo et al., 2013).

(Table 1). In addition to particulate trace metal pools, we also estimated dissolved trace metal fluxes by using the concentrations obtained near the Kuroshio region (Ren et al., 2015; Su et al., 2015; Wang et al., 2014). The results of the estimated dissolved and particulate metal fluxes are shown in Table 1. The dissolved fluxes for phosphate are generally threefold to fivefold higher than its total particulate fluxes, indicating that dissolved phosphate is the dominant pool in the water mass. For Al and Fe, their fluxes in the dissolved pool are twofold to threefold higher than the particulate pools. For all other trace metals, the dissolved fluxes are fivefold to tenfold higher than the particulate fluxes. These results indicate that the majority of trace metals transported in the Kuroshio region are dissolved but not particulate pools.

## 6. Sources of Particulate Trace Metals

Elemental ratios are useful indicators to elucidate the sources of particulate trace elements in the ocean because of the distinguishable elemental ratios existing in the composition of the end-member source materials. For example, by using their distinguishable P- or Al-normalized elemental ratios for biogenic and abiotic end-members, we previously demonstrated that anthropogenic aerosols are the major sources for most of particulate trace metals in the surface water of the SCS and WPS (Ho et al., 2007; Liao et al., 2017). We assumed that particulate trace metals in oceanic surface water are composed of three major sources: biogenic, lithogenic (aerosol and nonaerosol), and anthropogenic fractions. Total metal concentrations in size-fractionated suspended particles can thus be quantitatively expressed using a mass balance expression (equation (1)). As it is operationally difficult to differentiate aerosol Al from nonaerosol Al in samples, we sum these two abiotic fractions to simplify abiotic sources by using bulk particulate Al concentrations as shown in equation (2). The two-component formulas are further transformed into the formula normalized to  $[P]_t$  or  $[Al]_t$  (equation (3)) to exhibit the distribution pattern of P- or Al-normalized metal ratios and their closeness with the composition in the biotic and abiotic fractions (Figure 7).

$$[M]_t = a [Al]_a + b [Al]_l + c [P]_t \quad (1)$$

$$[M]_t = S [Al]_t + c [P]_t \quad (2)$$

$$[M]_t/[P]_t = S [Al]_t/[P]_t + c \text{ or } [M]_t/[Al]_t = S + c [P]_t/[Al]_t \quad (3)$$

- a*: averaged Al-normalized metal ratios in aerosols (shown as red lines in figures)
- b*: averaged Al-normalized metal ratios in nonaerosol lithogenic particles (blue lines)
- c*: P-normalized intracellular metal quota in plankton (green lines)
- S*: the slopes of the regression lines between M/P and Al/P

$[M]_t$ : total particulate metal concentration of individual element

$[Al]_a$ : Al concentration in anthropogenic aerosol particles

$[Al]_l$ : Al concentration in non-aerosol lithogenic particles

$[Al]_t$ : total particulate Al concentration

$[P]_t$ : total particulate P concentration

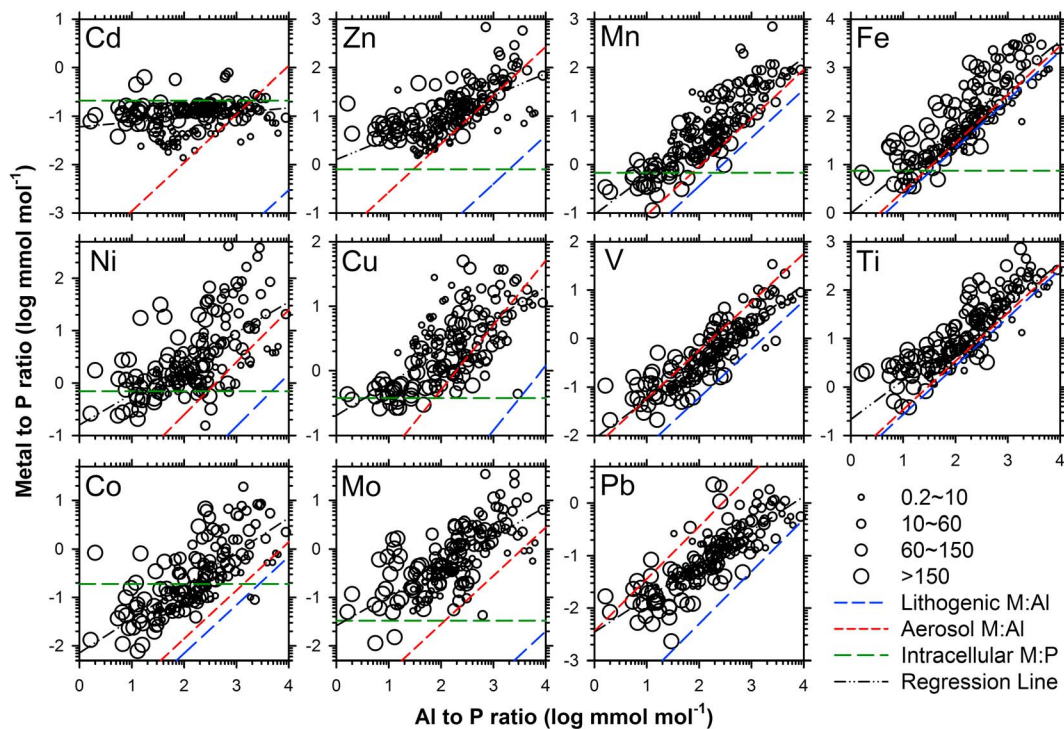


**Figure 7.** The distribution pattern of particulate metal to P ratios versus Al to P ratios (mmol/mol) in size-fractionated particles and their comparison with the reference ratios, including in situ aerosol metal to Al ratios obtained in the Western Philippine Sea, lithogenic metal to Al ratios, and intracellular metal to P quotas (Table 2). Black dash lines represent the regression lines of all data points for each element.

Particulate trace metal ratios in the samples are compared to the reference ratios of the three major components, including lithogenic particles, anthropogenic aerosols, and intracellular metal (Table 2). The averaged Al-normalized lithogenic ratios (a) were obtained from studies in East Asia (Hu & Gao, 2008). The averaged Al-normalized ratios in anthropogenic aerosols (b) were obtained from our previous study in the WPS (Liao et al., 2017). The M/Al ratios of anthropogenic aerosols obtained in the WPS are comparable to other studies in the ECS and Okinawa, indicating that the average values used are representative for this study (Table 2). The biogenic, or P-normalized intracellular quotas, are based on the value obtained from the averages of

**Table 2**  
The Reference Values of M/Al Ratios and Intracellular M/P Quotas Used in Figure 7

M/Al or M/P (mmol/mol <sup>-1</sup> )	Ti	V	Mn	Fe	Co	Ni	Cu	Zn	Pb	Cd	Mo
Aerosols (M/Al)											
WPS <sup>a</sup>	34	5.7	9.1	281	0.14	2.5	5.1	27	3.6	0.11	0.28
ECS <sup>b</sup>	42	3.3	12.8	322	0.19	1.1	40	34	3.6	0.20	0.16
Okinawa <sup>c</sup>	37	n.a.	15.3	285	0.17	3.5	1.4	21	2.7	0.18	n.a.
Lithogenic materials (M/Al)											
East Asia craton <sup>d</sup>	27	0.64	3.6	218	0.068	0.15	0.12	0.36	0.054	0.00027	0.0017
Biogenic materials (M/P)											
Intracellular quota <sup>e</sup>	n.a.	n.a.	0.68	7.5	0.19	0.70	0.38	0.80	n.a.	0.21	n.a.
Suspended particles (M/Al)											
Yangtze River <sup>f</sup>	37	n.a.	6.4	285	0.11	0.32	0.37	0.87	0.10	0.0019	n.a.
Yangtze River <sup>g</sup>	n.a.	n.a.	n.a.	248	0.12	0.35	0.31	0.80	0.09	0.0078	n.a.

*Note.* The elemental ratios are significantly different between the aerosols and the lithogenic material (Liao et al., 2017), except Fe and Ti. The ratios in aerosols and lithogenic material are  $281 \pm 68$  and  $218 \pm 92$  for Fe and  $34 \pm 6$  and  $27 \pm 12$  for Ti, respectively. WPS = Western Philippine Sea; ECS = East China Sea; n.a. = not applicable.

<sup>a</sup>Liao et al. (2017). <sup>b</sup>Hsu et al. (2010). <sup>c</sup>Okubo et al. (2013). <sup>d</sup>Compiled from Hu and Gao (2008). <sup>e</sup>Compiled from Ho et al. (2003) and Ho (2006). <sup>f</sup>Koshikawa et al. (2007). <sup>g</sup>Yuan et al. (2012).

representative culture and field studies (Ho, 2006; Ho et al., 2003). The regression lines between  $\log [M]_t/[P]_t$  and  $\log [Al]_t/[P]_t$  are also plotted to evaluate the association to the reference ratios (Figure 7). Using  $\log [M]_t/[P]_t$  as the y axes and  $\log [Al]_t/[P]_t$  as the x axes, the variability and distribution patterns of the elemental ratios are used to evaluate the relative contribution of abiotic or biotic components in the suspended particles (Figures 7 and S2). Based on the association of metal ratios to the reference lines (Figure 7), the elements investigated may be categorized into three groups: the elements closely associated with intracellular composition, including P and Cd, the elements closely associated with anthropogenic aerosols, including Zn, Cu, Ni, Co, V, Mn, Mo, and Pb, and the elements closely associated with both lithogenic materials and/or anthropogenic aerosols, including Al, Ti, and Fe. The vertical variations are also compared at different vertical layers, including the top 50 m, the Chl *a* maximum zone, and the depth at 150 or 200 m (Figure S2). In addition to the x-y plot, the contour of the ratios along the studied path are also plotted to exhibit their spatial variations (Figures S3 and S4).

Particulate Cd and P are known to be highly correlated with each other mainly due to biological uptake in the surface water (Ho et al., 2009; Quay et al., 2015). Comparable to PCA results, the Cd to P ratio distribution patterns are relatively consistent (Figure 7). Although the ratios are closely associated with intracellular Cd quota (Ho, 2006; Ho et al., 2003), most of the ratios are lower than the intracellular quota, especially for the samples in the smallest fraction, 0.2–10  $\mu\text{m}$ . The averaged Cd/P ratio in the fraction is  $0.05 \pm 0.02$  mmol/mol, which is significantly lower than the reference quota of 0.21 (Table 2). It should be noted that the averaged Cd to P reference line was mainly based on the average value for an eukaryotic phytoplankton culture study and some field studies which mainly collected relatively large phytoplankton (Ho, 2006). As suggested in our previous study (Liao et al., 2017), the discrepancy may be attributed to the dominance of *Prochlorococcus* and *Synechococcus* in the studied region (Chiang et al., 2002; Jiao et al., 2005) because the Cd quota observed in cyanobacteria (Cunningham & John, 2017) was much lower than the other eukaryotic phyla in our culture study (Ho et al., 2003). Lower Cd/P ratios in the SSF were also highly correlated with the Chl *a* concentrations in the surface water of the transect (Figures 2 and S3), supporting the argument that the low Cd/P ratios were attributed to the small size cyanobacteria. Attributed to the significantly different Cd to P ratios between the SSF and LSF, disproportional export of the SSF and LSF may influence dissolved Cd to P ratios in the deeper water. Among the metals studied, Ni and Co to P ratios in the LSF are also relatively close to the intracellular reference line. Although biogenic materials contribute a certain amount of Ni and Co into particles, their Al-normalized ratios are still above the aerosol reference lines, indicating that the Ni and Co in anthropogenic aerosols may also be a major source to particulate phase. The slope of regression line in the plot of Ni/P and Co/P versus Al/P (Figure 7) is 0.53 and 0.58, respectively, indicating that abiotic materials, mainly anthropogenic materials, are a major source of particulate Ni and Co.

Zn and Cu are elements with their ratio distribution patterns associated to both biotic and abiotic reference lines (Figure 7). Most of their Al-normalized and P-normalized ratios are significantly higher than the intracellular quota but relatively close to the aerosol M/Al ratios, implying that the metals were extracellularly adsorbed or aggregated on the biotic particles and the metals were originated from anthropogenic aerosols. This observation was similar to our previous study in the WPS (Liao et al., 2017). In the sectional distribution of the SSF (Figure S3), the M/P ratios were all relatively low in the high Chl *a* zone due to the increase of biomass or particulate P; their M/Al were thus elevated due to the decrease of abiotic fractions. The P-normalized Zn ratios for all size fractions were higher than the intracellular quota. Indeed, both Zn isotopic and elemental composition obtained from various oceanic basins have shown strong evidence of scavenging process for Zn cycling in marine water columns (John & Conway, 2014; Liao et al., 2017). Due to the high anthropogenic aerosol deposition in the surface water of the NWPO and its marginal seas, we proposed that the scavenging of aerosol Zn by phytoplankton in oceanic surface water is a dominant process for Zn cycling in the oceanic regions with high anthropogenic aerosol deposition (Ho et al., 2007; Liao et al., 2017). Ho et al. (2011) further demonstrated that Zn/Al and Zn/P ratios in sinking particles collected in the deep water of the SCS were significantly higher than the lithogenic ratios and intracellular quota, indicating that anthropogenic aerosol Zn have been transported to the deep water. As Zn isotopic composition is much lighter in anthropogenic materials than lithogenic particles (Mattielli et al., 2009), studies on Zn isotopic composition in dissolved and particulate phases may be used to quantify the relative contribution of anthropogenic particles in the deep water. For Cu in the size range larger than 150  $\mu\text{m}$ , the P-normalized ratios were fairly close to the intracellular quota, which may be attributed to the relatively low surface area to volume ratio in the samples,

which results in relatively low adsorption in the large particles. Mo showed a similar pattern with Cu and Zn, suggesting that the contribution of the anthropogenic material is significant. Indeed, fossil fuel combustion was reported to be a major Mo source in the surface ocean (Chappaz et al., 2012; Pacyna & Pacyna, 2001).

For Fe, Ti, and Mn, most of the data are slightly higher than or comparable to the two abiotic reference ratios,  $a$  and  $b$ . Their distribution pattern is also similar to what we observed in the SCS and the WPS (Ho et al., 2007; Liao et al., 2017). Anthropogenic aerosol deposition may contribute a significant amount of the metals to the particulate pool (Liao et al., 2017). However, as the difference between the two reference ratios of these three elements is relatively small (Figure 7), elemental ratios may not be a precise approach to quantify the relative contribution of the two abiotic sources. The other possible abiotic source may come from sediment resuspension through vertical turbulent mixing induced by flow-topography interactions (Figures 4 and 5). In addition to bottom up source, anthropogenic materials brought up by the horizontal transport of Yangtze River material may be the other important source in the region. Trace metals to Al ratios of suspended particles collected in Yangtze River were indeed higher than their lithogenic ratios, indicating anthropogenic material may be transported by riverine input to the studied region (Table 2) (Koshikawa et al., 2007; Yuan et al., 2012). Metal isotopic composition shall be used to distinguish their relative quantitative contribution of these various sources to the particulate metals.

Most of the V/Al ratios obtained from our particles are comparable to its aerosol reference line, showing that anthropogenic materials are the major sources of particulate V in the studied region. Although particulate V may also originate from bottom sedimentary suspension (Figure 4), their elemental ratios indicate that their sources mainly come from anthropogenic materials originated from either anthropogenic aerosols or riverine input (Yuan et al., 2012). In addition, our study area is located in a region of busy marine traffic, where fishing and cargo shipping activities are abundant. As aerosol V is known to be a major element in the flying ashes from heavy oil combustion (Becagli et al., 2012), the contribution of the heavy oil burning by fishing and cargo shipping would be a significant source in the studied region. For Pb, the other element whose source mainly originates from anthropogenic activities, its concentrations exhibit a unique distribution pattern (Figures 4 and 5). Pb does not have strong correlation with any other elements (Figure 6). It is known that anthropogenic aerosol input is the major source of elevated dissolved Pb concentrations observed in the ECS, which is about 1 order of magnitude higher than the concentrations in the Pacific (Chien et al., 2017; Lin et al., 2000). Due to its particle reactive characteristics, dissolved Pb originated from aerosol deposition would be quickly scavenged by particles.

Overall, except the upwelling region, the distribution patterns of all elemental ratios were similar to our previous observations in the WPS (Liao et al., 2017), indicating that anthropogenic aerosol deposition plays a major role for trace metal supply in the surface water of the Kuroshio adjacent to the ECS.

## 7. The Relationship Between Particulate Trace Metal Composition and Aerosol Deposition

Taking advantage of increasing particulate trace metal data sets available through GEOTRACES studies in global oceans, we have compared our data obtained in the NWPO and its marginal seas with the data obtained from other oceanic regions to examine the relationship of aerosol concentration variations with particulate trace metal composition in oceanic surface water (Table 3 and Figure 8). Using Cd, Fe, and Zn as representatives, the distribution patterns of their concentrations and slopes with P and Al for the samples collected in the top 200 m among different oceanic regions are shown in Figure 8. The oceanic regions include the North Atlantic Ocean (NAO), the Southeastern Pacific Ocean (SEPO), and the NWPO and its marginal seas. The NWPO data include the data obtained in the SCS (Ho et al., 2007), the WPS (Liao et al., 2017), and the Kuroshio region (this study), which are shown as red open circle, semifilled circle, and circle with cross in Figure 8, respectively. The SEPO data are from TN303 cruise, EPZT, GP16 (Ohnemus et al., 2017; Sherrell et al., 2016); and the NAO data are from KN199-04 and KN204-01 cruises, GA03 (Bourne et al., 2014; Lam, 2014; Lam et al., 2015; Ohnemus & Lam, 2015). For the SEPO study, the data were further separated into upwelling and nonupwelling regions by using phosphate concentrations higher than  $0.5 \mu\text{M}$  as cutoff (Ohnemus et al., 2017), which are shown as dark blue triangle symbols and purple triangle symbol with cross in Figure 8, respectively. The data set of the NWPO and its marginal seas include marginal sea (Ho et al., 2007), transition region from the ECS to the NWPO (this study), and the open ocean region in

**Table 3**  
Aerosol Fe and Zn Concentrations Reported in the Three Oceanic Regions Studied

Basin	Sampling information			Concentration (ng m <sup>-3</sup> ) <sup>a</sup>	
	Location	Time	Sample	Fe	Zn
NWPO	SCS <sup>b</sup>	July 2007	Bulk aerosol	246	82
	SCS <sup>b</sup>	October 2007		549	1241
	ECS <sup>c</sup>	2005–2007	Bulk aerosol	410	51
	Okinawa <sup>d</sup>	March–May 2008	Rain	98	35
	Honshu <sup>d</sup>			325	93
	Hokkaido <sup>d</sup>			112	25
	P02 (30°N 130–160°E) <sup>e</sup>	June–August 2004	Bulk aerosol	44	n.d. <sup>f</sup>
NAO	10–42°N 15–67°W <sup>g</sup>	May 1974	Bulk aerosol	100	4.3
	A16N <sup>h</sup>	June–August 2003	Bulk aerosol	217	n.d.
	5°S to 35°N 10–40°W <sup>i</sup>	2000–2011	Bulk aerosol and Rain	145	n.d.
	CVAO <sup>j</sup>	2007–2008	Bulk aerosol	450	4.3
	10–35°N 20–40°W <sup>j</sup>	January–February 2008		1250	6.2
SEPO	Samoa <sup>k</sup>	January–February 1981	Bulk aerosol (remote)	0.21	0.06
		July–August 1981	Bulk aerosol (local)	2.2	0.32
	P16 (0–25°S 150°W) <sup>e</sup>	January–February 2005	Bulk aerosol	2.3	n.d.
	Peru coast <sup>l</sup>	December 2012	Soluble	4.8	1.6

<sup>a</sup>We use 2 and 0.5 cm/s as the dry deposition velocity to convert fluxes to concentrations for Fe and Zn, respectively. NWPO = Northwestern Pacific Ocean; NAO = North Atlantic Ocean; SEPO = Southeastern Pacific Ocean; SCS = South China Sea; ECS = East China Sea; CVAO = Cape Verde Atmospheric Observatory. <sup>b</sup>Ho et al. (2010). <sup>c</sup>Hsu et al. (2010). <sup>d</sup>Okubo et al. (2013). <sup>e</sup>Buck et al. (2013). <sup>f</sup>n.d.: no data available. <sup>g</sup>Buat-Ménard and Chesselet (1979). <sup>h</sup>Buck et al. (2010). <sup>i</sup>Powell et al. (2015). <sup>j</sup>Patey et al. (2015). <sup>k</sup>Arimoto et al. (1987). <sup>l</sup>Baker et al. (2016).

the NWPO (Liao et al., 2017). We have demonstrated the dominant role of aerosol deposition on deciding trace metal composition in the suspended particles of the surface water either in the marginal seas or the open ocean region. The concentrations of Cd, Fe, and Zn in surface water suspended particles are compared with either the P or Al concentrations to examine their distribution patterns at various oceanic regions globally (Figure 8). The concentrations of Fe and Zn in aerosols are also compiled to exhibit the variations of trace metal concentrations among different oceanic regions (Table 3).

As expected, four Cd concentration data sets all show a relatively strong linear relationship with P among the three major oceanic regions, with linear correlation coefficients to be 0.60, 0.87, and 0.37 for the NWPO and its marginal seas, the SEPO, and the NAO, respectively. The Cd to P slopes in the NWPO and its marginal seas were overall slightly lower than the nonupwelling SEPO but higher than in the NAO, which are 0.100, 0.034, 0.068 mmol/mol to P for the nonupwelling SEPO, the NWPO and its marginal seas, and the NAO, respectively. On the other hand, the Cd/P ratios of the upwelling region in the SEPO is up to 0.84 mmol/mol ( $r = 0.88$ ), which may be attributed to the preferential uptake of Cd by diatom. For Cd to Al ratios, there are no significant linear relationships between Cd and Al among all of the data sets, simply showing that the contribution of abiotic particulate Cd is insignificant and particulate Al was not associated with phytoplankton at all (Figure 8).

In contrast to Cd, Fe concentrations possess a highly significant linear relationship with Al among all regions ( $r = 0.83$ ,  $p < 0.01$ , all data). However, there is no significant correlation observed between Fe and P for either individual oceanic region or all of the three data sets ( $r = 0.18$ ,  $p < 0.01$ ) although Fe is the most abundant essential trace metal biologically in plankton (Ho et al., 2003). These distribution patterns indicate that intracellular Fe only accounts for a very small fraction in total particulate Fe collected in the surface water of the major oceanic regions. These patterns also support the argument we have proposed in our previous studies that total particulate Fe samples collected in the euphotic zone of the SCS and WPS are mainly abiotic fraction, either adsorbed or aggregated on the surface of biotic particles or existing independently (Ho et al., 2007; Liao et al., 2017). Overall, the particulate Fe concentrations ranged from 0.03 to 30 nM in the surface waters (Figure 8). We also observed that variations of particulate Fe concentrations are positively correlated with variations of aerosol Fe concentrations or fluxes reported in the three major oceanic regions (Table 3). The deposited aerosol Fe concentrations in the NWPO and its marginal seas and the NAO are about 1 order of magnitude higher than the SEPO. For the SEPO nonupwelling region where aerosol deposition is low, we

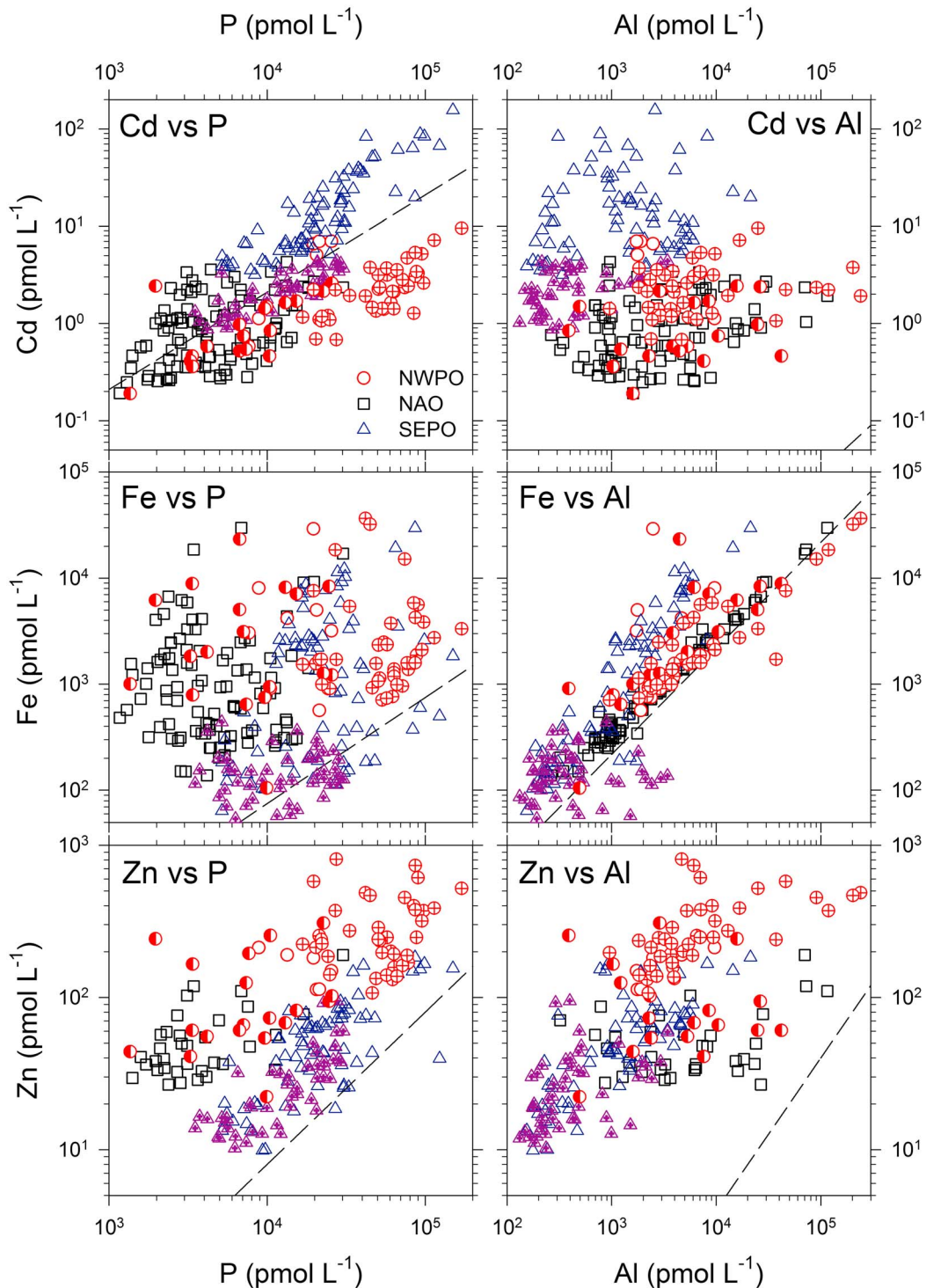


**Figure 8.** The distribution pattern of total concentrations of particulate Fe, Zn, and Cd in comparison with either particulate P or Al in the surface water of three major oceanic regions, the Northwestern Pacific Ocean (NWPO) and its marginal seas, the North Atlantic Ocean, and the Southeastern Pacific Ocean (SEPO). The data set of the NWPO and its marginal seas are composed of three data sets obtained from the South China Sea (red open circle), the Western Philippine Sea (red semifilled circle), and the Kuroshio region (red circle with cross). The SEPO data set is separated to upwelling (dark blue open triangle) and nonupwelling regions (purple open triangle with cross). The dash lines in the P comparison panel represent the metal intracellular quotas; the dash lines in the Al comparison panel represent the metal lithogenic ratios (Table 2). The North Atlantic Ocean samples were larger than 1  $\mu\text{m}$  and collected at 2 to 5 depths in top 200 m from 22 stations; the NWPO samples were larger than either 0.2 or 0.4  $\mu\text{m}$  and collected at 3 depths in top 200 m from 23 stations; and the SEPO samples were larger than 0.45  $\mu\text{m}$  and collected at 2 to 8 depths in top 200 m from 30 stations (Bourne et al., 2014; Lam, 2014; Lam et al., 2015; Ohnemus et al., 2017; Ohnemus & Lam, 2015; Sherrell et al., 2016). The sampling details may be found in the references cited.

also found that Fe to Al ratios are not linear at all but the Fe to P ratios for most of the samples are very close to the proposed intracellular ratios or ranges (Table 2). The contrasting and consistent distribution patterns between Cd and Fe among the datasets validate that most of particulate Fe collected in the surface water originate from abiotic materials in the oceanic regions with relatively high aerosol deposition, witnessed by the random concentration distribution with P.

Zn is representative for “hybride-type” elements, possessing relatively linear relationship with both P and Al. The linear correlation coefficients with P and Al are 0.42 and 0.59, respectively. The total particulate Zn concentrations are in the sequence of NWPO  $\gg$  NAO  $\sim$  SEPO<sub>upwelling</sub>  $>$  SEPO<sub>nonupwelling</sub>. The particulate Zn concentrations in the surface water of the NWPO and its marginal seas were roughly one order of magnitude higher than the NAO, also positively correlated to the difference for aerosol deposition fluxes observed in the two oceanic regions (Table 3). Comparable to Fe, for data obtained in the nonupwelling SEPO region where external input is extremely low (Table 3), Zn to P ratios are relatively close to its intracellular quota proposed and Zn to Al ratios are highly deviated from its lithogenic ratio (Figure 8). This distribution pattern again validates trace metal stoichiometric concept in plankton proposed (Ho, 2006; Ho et al., 2003). The relatively positive correlation between particulate Zn and P but highly enriched Zn/P ratios for most of the data indicates that particulate Zn is mainly extracellularly adsorbed or aggregated on biotic particles in the surface water. Figure 8 shows that, either at the extremely high or extremely low aerosol deposition regions, the distribution of the elemental ratios exhibits a consistent pattern globally. The globally consistent correlation between aerosol concentrations and total particulate trace metal composition supports our previous arguments that extracellular adsorption and/or aggregation is a major process on scavenging aerosol Zn and some other trace metals not only in the surface ocean of the NWPO and its marginal seas but also in other open ocean regions, particularly the oceanic regions in Northern Hemisphere where aerosol depositions are relatively high (Liao et al., 2017).

## 8. Conclusion

This study investigated trace metal composition and their elemental distribution pattern in size-fractionated particles collected in the surface water of the Kuroshio along the ECS. We found that anthropogenic aerosol deposition is the dominant source of particulate trace metal concentrations in the Kuroshio region, similar to what we have observed in the SCS and the WPS. The consistent distribution pattern of particulate trace metals observed in the NWPO and its marginal seas and other oceanic regions indicates that aerosol deposition is a controlling factor for particulate trace metal composition in the surface ocean globally. Future studies should comprehensively investigate the elemental and isotopic composition of trace metals in aerosols, seawater, and particles to fully elucidate how aerosol metals are internally cycled in marine water column.

## References

- Arimoto, R., Duce, R. A., Ray, B. J., Hewitt, A. D., & Williams, J. (1987). Trace elements in the atmosphere of American Samoa: Concentrations and deposition to the tropical South Pacific. *Journal of Geophysical Research*, 92(D7), 8465–8479. <https://doi.org/10.1029/JD092iD07p08465>
- Atkinson, L. P. (2010). Western boundary currents. In K.-K. Liu, L. Atkinson, R. Quiñones, & L. Talaue-McManus (Eds.), *Carbon and nutrient fluxes in continental margins: A global synthesis* (pp. 121–169). Berlin, Heidelberg, Springer Berlin Heidelberg. [https://doi.org/10.1007/978-3-540-92735-8\\_3](https://doi.org/10.1007/978-3-540-92735-8_3)
- Baker, A. R., Thomas, M., Bange, H. W., & Plasencia Sánchez, E. (2016). Soluble trace metals in aerosols over the tropical south-east Pacific offshore of Peru. *Biogeosciences*, 13(3), 817–825. <https://doi.org/10.5194/bg-13-817-2016>
- Becagli, S., Sferlazzo, D. M., Pace, G., di Sarra, A., Bommarito, C., Calzolari, G., et al. (2012). Evidence for heavy fuel oil combustion aerosols from chemical analyses at the island of Lampedusa: A possible large role of ships emissions in the Mediterranean. *Atmospheric Chemistry and Physics*, 12(7), 3479–3492. <https://doi.org/10.5194/acp-12-3479-2012>
- Bishop, J. K. B., Edmond, J. M., Ketten, D. R., Bacon, M. P., & Silker, W. B. (1977). The chemistry, biology, and vertical flux of particulate matter from the upper 400 m of the equatorial Atlantic Ocean. *Deep Sea Research*, 24(6), 511–548. [https://doi.org/10.1016/0146-6291\(77\)90526-4](https://doi.org/10.1016/0146-6291(77)90526-4)
- Bourne, H., Bishop, J. K. B., & Wood, T. (2014). *Global spatial and temporal variation of Cd:P in euphotic zone particulates. Paper presented at 47th Fall Meeting*. San Francisco, CA: American Geophysical Union.
- Buat-Menard, P., & Chesselet, R. (1979). Variable influence of the atmospheric flux on the trace metal chemistry of oceanic suspended matter. *Earth and Planetary Science Letters*, 42(3), 399–411. [https://doi.org/10.1016/0012-821X\(79\)90049-9](https://doi.org/10.1016/0012-821X(79)90049-9)
- Buck, C. S., Landing, W. M., & Resing, J. (2013). Pacific Ocean aerosols: Deposition and solubility of iron, aluminum, and other trace elements. *Marine Chemistry*, 157, 117–130. <https://doi.org/10.1016/j.marchem.2013.09.005>
- Buck, C. S., Landing, W. M., Resing, J., & Measures, C. (2010). The solubility and deposition of aerosol Fe and other trace elements in the North Atlantic Ocean: Observations from the A16N CLIVAR/CO2 repeat hydrography section. *Marine Chemistry*, 120(1–4), 57–70. <https://doi.org/10.1016/j.marchem.2008.08.003>

## Acknowledgments

We thank Jing Zhang for leading the Japan GEOTRACES cruise (KH-15-3) and the crew members and participants in the R/V Hakuho-Marui cruise for their assistance on seawater sampling and onboard measurement for hydrographic parameters. We also thank Yi-Chia Hsin for providing Kuroshio velocity information, Chih-Chiang Hsieh and Wan-Chen Tu for their assistance on measuring trace metal concentrations, and Shun-Chung Yang and Shotaro Takano for their helpful comments and discussions on this study. The raw data of this study in the Kuroshio can be found in the supporting information. We thank Phoebe Lam, Daniel Ohnemus, Benjamin Twining, and Robert Sherrell for sharing the published data obtained in the NAO and SEPO regions. The raw data can be found in <https://www.bco-dmo.org/dataset/639847/data> and <https://www.bco-dmo.org/dataset/3871/data>. The financial support of this study mainly came from Taiwan Ministry of Science and Technology grant 105-2119-M-001-039-MY3 and Career Development Award of Tung-Yuan Ho from Academia Sinica, and partially from Japan GEOTRACES program.

- Burd, A. B., Moran, S. B., & Jackson, G. A. (2000). A coupled adsorption–aggregation model of the POC/<sup>234</sup>Th ratio of marine particles. *Deep Sea Research, Part I*, 47(1), 103–120. [https://doi.org/10.1016/S0967-0637\(99\)00047-3](https://doi.org/10.1016/S0967-0637(99)00047-3)
- Chang, M.-H., Tang, T. Y., Ho, C.-R., & Chao, S.-Y. (2013). Kuroshio-induced wake in the lee of Green Island off Taiwan. *Journal of Geophysical Research: Oceans*, 118, 1508–1519. <https://doi.org/10.1002/jgrc.20151>
- Chao, S.-Y. (1991). Circulation of the East China Sea, a numerical study. *Journal of Oceanography*, 46(6), 273–295. <https://doi.org/10.1007/bf02123503>
- Chappaz, A., Lyons, T. W., Gordon, G. W., & Anbar, A. D. (2012). Isotopic fingerprints of anthropogenic molybdenum in lake sediments. *Environmental Science and Technology*, 46(20), 10,934–10,940. <https://doi.org/10.1021/es3019379>
- Chen, C.-C., Jan, S., Kuo, T.-H., & Li, S.-Y. (2017). Nutrient flux and transport by the Kuroshio east of Taiwan. *Journal of Marine Systems*, 167, 43–54. <https://doi.org/10.1016/j.jmarsys.2016.11.004>
- Chiang, K.-P., Kuo, M.-C., Chang, J., Wang, R.-H., & Gong, G.-C. (2002). Spatial and temporal variation of the *Synechococcus* population in the East China Sea and its contribution to phytoplankton biomass. *Continental Shelf Research*, 22(1), 3–13. [https://doi.org/10.1016/S0278-4343\(01\)00067-X](https://doi.org/10.1016/S0278-4343(01)00067-X)
- Chien, C. T., Ho, T.-Y., Sanborn, M. E., Yin, Q. Z., & Paytan, A. (2017). Lead concentrations and isotopic compositions in the Western Philippine Sea. *Marine Chemistry*, 189, 10–16. <https://doi.org/10.1016/j.marchem.2016.12.007>
- Cunningham, B. R., & John, S. G. (2017). The effect of iron limitation on cyanobacteria major nutrient and trace element stoichiometry. *Limnology and Oceanography*, 62(2), 846–858. <https://doi.org/10.1002/lno.10484>
- Guo, X., Zhu, X.-H., Long, Y., & Huang, D. J. (2013). Spatial variations in the Kuroshio nutrient transport from the East China Sea to south of Japan. *Biogeosciences*, 10(10), 6403–6417. <https://doi.org/10.5194/bg-10-6403-2013>
- Hasegawa, D., Yamazaki, H., Ishimaru, T., Nagashima, H., & Koike, Y. (2008). Apparent phytoplankton bloom due to island mass effect. *Journal of Marine Systems*, 69(3–4), 238–246. <https://doi.org/10.1016/j.jmarsys.2006.04.019>
- Ho, T.-Y. (2006). The trace metal composition of marine microalgae in cultures and natural assemblages. In D. V. Subba Rao (Ed.), *Algal cultures: Analogues of blooms and applications* (pp. 271–299). Enfield, NH: Science Publishers.
- Ho, T.-Y., Chou, W.-C., Lin, H.-L., & Sheu, D. D. (2011). Trace metal cycling in the deep water of the South China Sea: The composition, sources, and fluxes of sinking particles. *Limnology and Oceanography*, 56(4), 1225–1243. <https://doi.org/10.4319/lno.2011.56.4.1225>
- Ho, T.-Y., Chou, W.-C., Wei, C.-L., Lin, F.-J., Wong, G. T. F., & Lin, H.-L. (2010). Trace metal cycling in the surface water of the South China Sea: Vertical fluxes, composition, and sources. *Limnology and Oceanography*, 55(5), 1807–1820. <https://doi.org/10.4319/lno.2010.55.5.1807>
- Ho, T.-Y., Quigg, A., Finkel, Z. V., Milligan, A. J., Wyman, K., Falkowski, P. G., & Morel, F. M. M. (2003). The elemental composition of some marine phytoplankton. *Journal of Phycology*, 39(6), 1145–1159. <https://doi.org/10.1111/j.0022-3646.2003.03-090.x>
- Ho, T.-Y., Wen, L.-S., You, C.-F., & Lee, D.-C. (2007). The trace metal composition of size-fractionated plankton in the South China Sea: Biotic versus abiotic sources. *Limnology and Oceanography*, 52(5), 1776–1788. <https://doi.org/10.4319/lno.2007.52.5.1776>
- Ho, T.-Y., You, C.-F., Chou, W.-C., Pai, S.-C., Wen, L.-S., & Sheu, D. D. (2009). Cadmium and phosphorus cycling in the water column of the South China Sea: The roles of biotic and abiotic particles. *Marine Chemistry*, 115(1–2), 125–133. <https://doi.org/10.1016/j.marchem.2009.07.005>
- Hsin, Y.-C., Wu, C.-R., & Shaw, P.-T. (2008). Spatial and temporal variations of the Kuroshio east of Taiwan, 1982–2005: A numerical study. *Journal of Geophysical Research*, 113, C04002. <https://doi.org/10.1029/2007JC004485>
- Hsu, S.-C., Wong, G. T. F., Gong, G.-C., Shiah, F.-K., Huang, Y.-T., Kao, S.-J., et al. (2010). Sources, solubility, and dry deposition of aerosol trace elements over the East China Sea. *Marine Chemistry*, 120(1–4), 116–127. <https://doi.org/10.1016/j.marchem.2008.10.003>
- Hu, Z., & Gao, S. (2008). Upper crustal abundances of trace elements: A revision and update. *Chemical Geology*, 253(3–4), 205–221. <https://doi.org/10.1016/j.chemgeo.2008.05.010>
- Jan, S., Yang, Y. J., Wang, J., Mensah, V., Kuo, T.-H., Chiou, M.-D., Chern C.S., Chang M.H., Chien H. (2015). Large variability of the Kuroshio at 23.75°N east of Taiwan. *Journal of Geophysical Research: Oceans*, 120, 1825–1840. <https://doi.org/10.1002/2014JC010614>
- Jiao, N., Yang, Y., Hong, N., Ma, Y., Harada, S., Koshikawa, H., & Watanabe, M. (2005). Dynamics of autotrophic picoplankton and heterotrophic bacteria in the East China Sea. *Continental Shelf Research*, 25(10), 1265–1279. <https://doi.org/10.1016/j.csr.2005.01.002>
- John, S. G., & Conway, T. M. (2014). A role for scavenging in the marine biogeochemical cycling of zinc and zinc isotopes. *Earth and Planetary Science Letters*, 394, 159–167. <https://doi.org/10.1016/j.epsl.2014.02.053>
- Koshikawa, M. K., Takamatsu, T., Takada, J., Zhu, M., Xu, B., Chen, Z., et al. (2007). Distributions of dissolved and particulate elements in the Yangtze estuary in 1997–2002: Background data before the closure of the Three Gorges Dam. *Estuarine, Coastal and Shelf Science*, 71(1–2), 26–36. <https://doi.org/10.1016/j.eccs.2006.08.010>
- Lam, P. J. (2014). Size-fractionated major and minor particle composition and concentration from R/V Knorr KN199-04, KN204-01 in the subtropical North Atlantic Ocean from 2010–2011 (U.S. GEOTRACES NAT project). Biological and Chemical Oceanography Data Management Office (BCO-DMO). Dataset version 2014-12-12 [Total particulate P, Al, Fe, Zn, and Cd concentrations in the TOP 200 m]. <http://lod.bco-dmo.org/id/dataset/3871> [2018–01]
- Lam, P. J., & Bishop, J. K. B. (2008). The continental margin is a key source of iron to the HNLC North Pacific Ocean. *Geophysical Research Letters*, 35, L07608. <https://doi.org/10.1029/2008GL033294>
- Lam, P. J., Ohnemus, D. C., & Auro, M. E. (2015). Size-fractionated major particle composition and mass from the US GEOTRACES North Atlantic Zonal Transect. *Deep Sea Research, Part II*, 116, 303–320. <https://doi.org/10.1016/j.dsr2.2014.11.020>
- Liao, W.-H., Yang, S.-C., & Ho, T.-Y. (2017). Trace metal composition of size-fractionated plankton in the Western Philippine Sea: The impact of anthropogenic aerosol deposition. *Limnology and Oceanography*, 62(5), 2243–2259. <https://doi.org/10.1002/lno.10564>
- Lin, F.-J., Hsu, S.-C., & Jeng, W.-L. (2000). Lead in the southern East China Sea. *Marine Environmental Research*, 49(4), 329–342. [https://doi.org/10.1016/S0141-1136\(99\)00076-8](https://doi.org/10.1016/S0141-1136(99)00076-8)
- Maranon, E. (2015). Cell size as a key determinant of phytoplankton metabolism and community structure. *Annual Review of Marine Science*, 7(1), 241–264. <https://doi.org/10.1146/annurev-marine-010814-015955>
- Mattielli, N., Petit, J. C. J., Deboudt, K., Flament, P., Perdrix, E., Taillez, A., et al. (2009). Zn isotope study of atmospheric emissions and dry depositions within a 5 km radius of a Pb–Zn refinery. *Atmospheric Environment*, 43(6), 1265–1272. <https://doi.org/10.1016/j.atmosenv.2008.11.030>
- Ohnemus, D. C., & Lam, P. J. (2015). Cycling of lithogenic marine particulates in the US GEOTRACES North Atlantic Zonal Transect. *Deep Sea Research, Part II*, 116, 283–302. <https://doi.org/10.1016/j.dsr2.2014.11.019>
- Ohnemus, D. C., Rauschenberg, S., Cutter, G. A., Fitzsimmons, J. N., Sherrell, R. M., & Twining, B. S. (2017). Elevated trace metal content of prokaryotic communities associated with marine oxygen deficient zones. *Limnology and Oceanography*, 62(1), 3–25. <https://doi.org/10.1002/lno.10363>
- Okubo, A., Takeda, S., & Obata, H. (2013). Atmospheric deposition of trace metals to the western North Pacific Ocean observed at coastal station in Japan. *Atmospheric Research*, 129–130, 20–32. <https://doi.org/10.1016/j.atmosres.2013.03.014>

- Pacyna, J. M., & Pacyna, E. G. (2001). An assessment of global and regional emissions of trace metals to the atmosphere from anthropogenic sources worldwide. *Environmental Review*, 9(4), 269–298. <https://doi.org/10.1139/a01-012>
- Patey, M. D., Achterberg, E. P., Rijkenberg, M. J., & Pearce, R. (2015). Aerosol time-series measurements over the tropical Northeast Atlantic Ocean: Dust sources, elemental composition and mineralogy. *Marine Chemistry*, 174, 103–119. <https://doi.org/10.1016/j.marchem.2015.06.004>
- Powell, C. F., Baker, A. R., Jickells, T. D., Bange, H. W., Chance, R. J., & Yodanis, C. (2015). Estimation of the atmospheric flux of nutrients and trace metals to the eastern tropical North Atlantic Ocean. *Journal of the Atmospheric Sciences*, 72(10), 4029–4045. <https://doi.org/10.1175/jas-d-15-0011.1>
- Quay, P., Cullen, J., Landing, W., & Morton, P. (2015). Processes controlling the distributions of Cd and PO<sub>4</sub> in the ocean. *Global Biogeochemical Cycles*, 29(6), 830–841. <https://doi.org/10.1002/2014gb004998>
- Ren, J.-L., Xuan, J.-L., Wang, Z.-W., Huang, D., & Zhang, J. (2015). Cross-shelf transport of terrestrial Al enhanced by the transition of north-easterly to southwesterly monsoon wind over the East China Sea. *Journal of Geophysical Research: Oceans*, 120, 5054–5073. <https://doi.org/10.1002/2014JC010655>
- Sherrell, R. M., Twining, B. S., & German, C. (2016). Trace elements in suspended particles from GO-Flo bottles. Biological and Chemical Oceanography Data Management Office (BCO-DMO). Dataset version 2016-05-17 [Total particulate P, Al, Fe, Zn, and Cd concentrations in the top 200 m]. <http://lod.bco-dmo.org/id/dataset/639847> [2018–01]
- Shiozaki, T., Takeda, S., Itoh, S., Kodama, T., Liu, X., Hashihama, F., & Furuya, K. (2015). Why is *Trichodesmium* abundant in the Kuroshio? *Biogeosciences*, 12(23), 6931–6943. <https://doi.org/10.5194/bg-12-6931-2015>
- Su, H., Yang, R. J., Zhang, A. B., & Li, Y. (2015). Dissolved iron distribution and organic complexation in the coastal waters of the East China Sea. *Marine Chemistry*, 173, 208–221. <https://doi.org/10.1016/j.marchem.2015.03.007>
- Tsutsumi, E., Matsuno, T., Lien, R.-C., Nakamura, H., Senjyu, T., & Guo, X. (2017). Turbulent mixing within the Kuroshio in the Tokara Strait. *Journal of Geophysical Research: Oceans*, 122, 7082–7094. <https://doi.org/10.1002/2017jc013049>
- Wang, B.-S., Lee, C.-P., & Ho, T.-Y. (2014). Trace metal determination in natural waters by automated solid phase extraction system and ICP-MS: The influence of low level Mg and Ca. *Talanta*, 128, 337–344. <https://doi.org/10.1016/j.talanta.2014.04.077>
- Wen, L.-S., Lee, C.-P., Lee, W.-H., & Chuang, A. (2018). An ultra-clean multilayer apparatus for collecting size fractionated marine plankton and suspended particles. *Journal of Visualized Experiments*, 134(134), e56811. <https://doi.org/10.3791/56811>
- Yuan, X., Li, J., Mao, C., Ji, J., & Yang, Z. (2012). Geochemistry of water and suspended particulate in the lower Yangtze River: Implications for geographic and anthropogenic effects. *International Journal of Geosciences*, 03(01), 81–92. <https://doi.org/10.4236/ijg.2012.31010>